THE JOURNAL OF PHYSICAL CHEMISTRY B

Article

pubs.acs.org/JPCB

Formation of Circular Crack Pattern in Deposition Self-Assembled by Drying Nanoparticle Suspension

Guangyin Jing*[,†,‡] and Jun Ma*[,†]

[†]Department of Physics, Northwest University, Xian 710069, China

[‡]NanoBiophotonics Center, National Key Laboratory and Incubation Base of Photoelectric Technology and Functional Materials, Xian 710069, China

Supporting Information

ABSTRACT: Curved cracks widely exist in nanoparticle (NP) deposition produced by drying colloidal suspension. Circular cracks, for example, initiate and propagate along a circular trajectory. One feasible theoretical explanation of a circular crack is the Xia-Hutchinson model, in which a preexisting track (flaw loop) in the film is necessary for initiating and propagating the crack on the circular path. Here, we report the first experimental evidence of dried deposition to support this model. Our results indicate that cracks along the circular trajectory can surprisingly "pass" across a 180 μm air gap. Moreover, two arc-path cracks originate in different areas and propagate to meet, forming a circular trajectory. These unexpected crack initiation and propagation indicate that the crack propagates alone the "preformed" track, experimentally confirming the hypothesis proposed by the Xia−Hutchinson model. The transition of the circular crack to a radial one indicates that the deposition microstructure is the dominant factor for the crack formation.

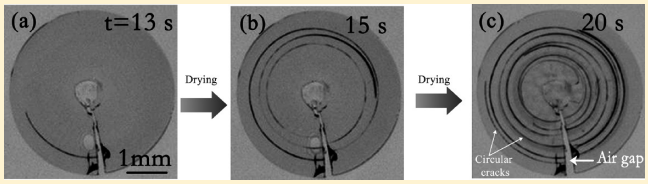

INTRODUCTION

Nanoparticle (NP) self-assembly is a key bottom-up nanofabrication approach in nanotechnology, which is achieved by drying NP suspension in nanofluid under the specific conditions. This sophisticated technology has been widely applied in the micro-/nanomanufacture of electronic structure,[1] the thin-film electrode of a battery,[2] photonic crystals,[3] and coating with a nanothickness,[4] etc. However, a critical problem significantly hinders those applications: cracks ubiquitously exist in the self-assembled structures formed by dried NPs, which greatly lowers and even damages the performance of these materials. Therefore, preventing or depressing the crack initiation and propagation is the prior task in those applicable areas, which relies on the understanding of the intrinsic mechanism of crack formation.

Intriguing curved crack trajectories formed on the dried deposition produced by drying a colloidal suspension, which displayed versatile morphologies under various experimental conditions: circle,[5] spiral,[6−9] wavy,[10] arch shape,[11] and irregular curve.[5] Circular cracks have been produced by drying the suspension drop of aqueous silica sols with high salt content.[5] The spiral crack path was captured in situ in drying gel film[12] and precipitate,[8] which exhibited an inward logarithmic spiral. Recently, Goehring et al.[10] experimentally demonstrated a wavy crack formation by drying a particle suspension.

By analysis of the fracture mechanism, Russel's pioneering works advanced the understanding of cracks on colloidal deposition.[13−15] For curved cracks, Xia and Hutchinson[16] supposed that there existed a preexisting track (flaw loop) in the film on which the crack formed; thereafter, they could explain the production of curved cracks by the fracture mechanism. However, this proposal needs to be confirmed by the evident experiments.

Motivated by the purpose of understanding the mechanism of a curved crack, drying of sessile aqueous drops with silica NP dispersion is employed for studying the curved cracks. We report here the first experimental evidence to support the assumption proposed by Xia and Hutchinson in their theoretical model.

EXPERIMENTAL SECTION

The suspension of silica NPs (~75 nm diameter, the polydispersity of the typical coefficient of variation (the ratio of the standard deviation to the mean) ≤ 10%, KLEBOSOL, AZ Electronic Materials) with the original mass fraction of 0.53 is diluted to different concentrations for the experiments. Deionized (DI) water (18.2 MΩ·cm) is used for the cleaning procedures and the dilution of silica suspension. A new plastic Petri dish of polystyrene is used once as the hydrophobic substrate in the drying experiment. Glass slides used as another type of substrate are cleaned by the typical Piranha procedure. These slides are immersed into the mixture solution of H_2SO_4 (98%) and H_2O_2 (30%) with the ratio of 3:7 at ~100 °C for 20 min, then rinsed several times with DI water, and dried by a stream of nitrogen. The clean glass plate is hydrophilic with a

Received: February 25, 2012
Revised: May 12, 2012
Published: May 12, 2012

water contact angle less than 5° after this cleaning procedure and is used for the drying experiment immediately.

The imaging system includes two CCD cameras: one is placed vertically for the top-view observation (Marlin F131B + Nikor 60 Mirco lens), and the other one is set horizontally for the side-view observation (Marlin F201B + Nikor 60 Mirco lens). These cameras are connected with the computer by the connector and software. After the cleaning procedure, the drops of suspension are immediately transferred from the solutions onto the clean glass slide or polystyrene dish. The cameras are then focused on the drop both vertically and horizontally, for the purpose of capturing image sequences. These drops are naturally drying in the ambient condition (temperature (T), 31 °C; relative humidity (RH), 37%). In general, the drying processes last for about 10 min on the glass plate and slightly longer than 30 min on the polystyrene one. It is checked that the environmental temperature and the humidity are reasonably stable during the drying process (±1 °C and ±1% RH, respectively).

RESULTS AND DISCUSSION

Results. *A. Circular Cracks Origin and Propagation. a. Circular Crack.* A drop of NP suspension (mass fraction, 0.35) with the contact angle of 55° dries on a hydrophobic polystyrene substrate (video in the Supporting Information). The diameter of the contact area of the drop with the substrate is 4.2 mm. As the drying front reaches the initial drop center, the gelation nearly finishes. The dried NP deposit consists of a circular disk, and the first crack in the radial direction appears and quickly propagates from the disk perimeter toward the center (Figure 1a). Afterward, an arc-path crack originates

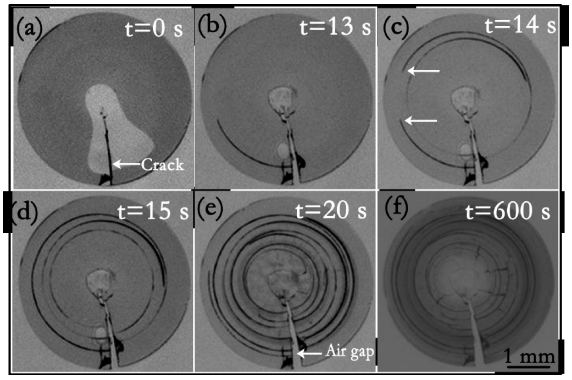

Figure 1. Formation and evolution of circular crack pattern on the polystyrene substrate. Mass fraction of NP suspension: 0.35. (a) A radial direction crack first appears. (b) A crack with an arc path originates. (c) More arc-path cracks are produced. Two cracks (arrows) with an arc path on a circular trajectory are separated by the continuous deposition. (d) Two separated curved cracks in c are connected by the crack propagation along a circular trajectory. An additional arc-path crack simultaneously develops in the inner area. (e) More and more cracks form toward the inner area. (f) The crack development finishes. A crack pattern with sets of circular cracks matures. The bar is 1 mm for all micrographs.

(Figure 1b). Only 1 s later, more arc-path cracks are produced, and two outer cracks with arc path are separated by a continuous deposit (indicated by the arrows in Figure 1c). After another 1 s, with the crack propagating, surprisingly, those two separated curved cracks subsequently meet and connect, constituting a circular trajectory (Figure 1d), as if cracks pass through a "preformed" track. Later several sets of circular cracks have developed (Figure 1e,f). More interestingly, the crack trajectory makes up a circle loop "across" an air gap (indicated by the arrow in Figure 1e) produced by the first radial crack. The maximum air gap "passed" by the circular crack has the extraordinary width of 180 μm. This illustrates that the formation of circular cracks does not really rely on the crack propagation but depends on the preformed trajectory. The circular crack path perpendicularly intersects to the first radial crack. Few theoretical works can successfully explain the circular crack besides the Xia–Hutchinson theory. The preformed track in the present work experimentally confirms the hypothesis proposed by the Xia–Hutchinson model; i.e., a crack with a circular trajectory propagates along the preexisting track (flaw loop) in the film.

b. Circular Cracks Accompanying the Radial Cracks. A drop suspension of contact angle 55° and diameter 2.4 mm dries on the polystyrene substrate, with the mass fraction of the NPs lowering to 0.20. Similar to the case in section A.a, a radius-directional crack first appears (Figure 2a). Multiple radial

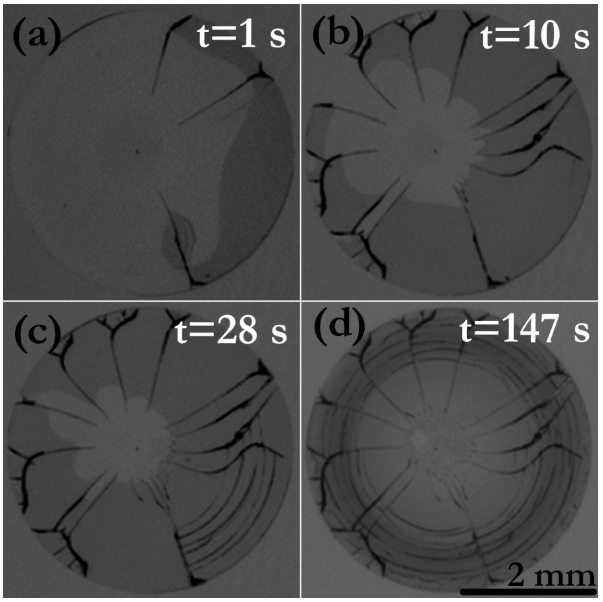

Figure 2. Pattern formation of the mixture of radius-directional and curved cracks on the polystyrene substrate. Mass fraction of NP suspension: 0.20. (a) Straight radius-directional cracks initiate at the beginning. (b) More straight radius-directional cracks form, accompanied by a few deformed radius-directional cracks. (c) With continued drying, sets of arc-path cracks come into being separated by some distance from each other. (d) Cracks with circular-like trajectories form at the end of the drying. The bar is 2 mm for all micrographs.

cracks subsequently form to separate the whole deposit disk into several sectors (Figure 2b). With the process proceeding, the arc-path cracks first appear in the lower right sector of the disk (Figure 2c); then more arc cracks are produced in all sectors (Figure 2d). Although there are many air gaps caused by radial cracks, the arc paths of cracks can still "meet" to make up entire circular trajectories, suggesting that the crack propagates on a preformed track in the deposition. This scenario further confirms the proposal in the Xia–Hutchinson model. The crack pattern demonstrates the mixture character of the radial cracks and circular ones. Due to all experimental

dx.doi.org/10.1021/jp301872r | J. Phys. Chem. B 2012, 116, 6225–6231

conditions being unchanged except the concentration, this pattern transition might be induced by the lower NP concentration.

c. Analysis of the Circular Cracks. Drying a series of NP suspension by varying the concentrations, similar circular cracks form and pass across the air gap in the NP deposition (Figure 3). As shown in Figure 3, more radial cracks are able to form by

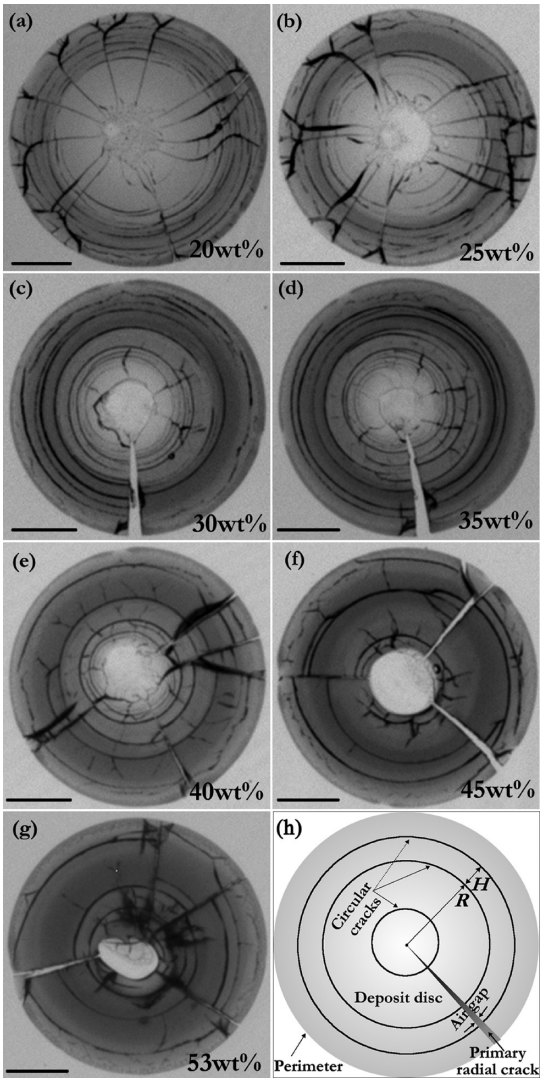

Figure 3. Crack patterns on the polystyrene substrate with various mass fractions of NP suspension: (a–g) optical micrograph of circular cracks on NP deposition produced by various NP mass fraction; (h) illustration of circular crack propagation across the air gap. The scale bar is 1 mm for all panels.

drying suspension drops with lower (<30%, Figure 3a,b) or higher (>40%, Figure 3e–g) concentrations, whereas less are produced with mediate concentrations (30 and 35%, Figure 3c,d). For the crack propagation across the air gap, the cases in Figure 3c,d are the kind analyzed in section A.a, and the remaining cases (Figure 3a,b,e–g) correspond to the other kind in section A.b. As displayed in Figure 4a, the *average* radius of circular cracks shows the decreasing tendency with the increase of NP mass fraction. The maximum radii for *all* NP mass fractions decrease from 2.0 to 1.4 mm with NP mass fraction increasing from 0.20 to 0.40. The difference between the maximum and minimum radii for *each* mass fraction ranges

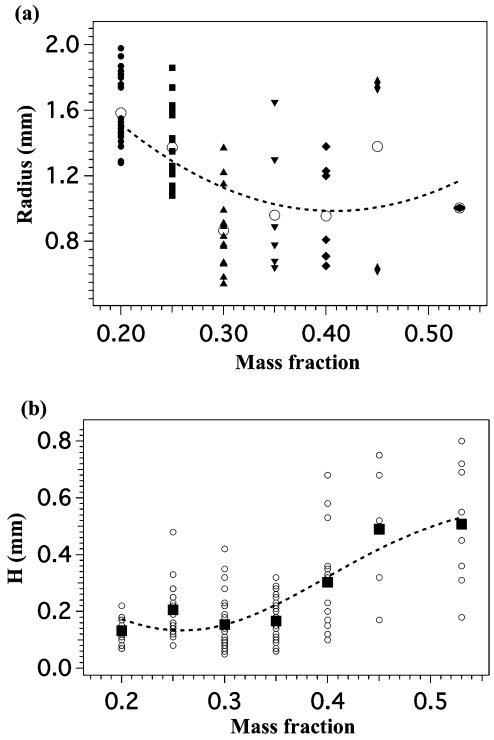

Figure 4. Radius (R) and the distance between adjacent cracks (H) versus mass fraction: (a) radius of circular crack; (b) crack distance dependence of NP mass fraction. (○, ■) Mean value for each mass fraction corresponding to a and b, respectively. The dashed line for the mean value in a is a three-term polynomial and in b is the Gaussian fitting. The error bars of R and H are ±0.01 mm.

from 0.7 to 1.1 mm, showing no dependence on the variation of the concentration. For all NP mass fractions, the ratio of the minimum radius to the maximum one is 1/4 (0.5 mm/2.0 mm). As the NP mass fractions increase, the *average* distance H between two adjacent circular cracks increases linearly, and its value fluctuates in a range from 0.1 to 0.5 mm (Figure 4b).

Interestingly, the numbers of cracks across the air gap reduce linearly with NP mass fraction increasing from 0.20 to 0.45: that is from 21 to 3 (Figure 5a). On the other hand, the mean thickness h of the NP deposition displays approximately linear growth with the increment of NP mass fractions (Figure 5b; $h = V/\pi r^2$, with V being the deposition volume and r the radius of the deposition disk). As shown in Figure 5c, for the deposition with thin thickness, the numbers of circular cracks across the air gap linearly decrease with the growth of the mean thickness of NP deposition. Obviously, increasing deposition thickness hinders the production of a crack, which is reasonable since making new interfaces by the crack consumes more energy in a thicker deposition.

As shown in Figure 3, crack patterns consist of concentric circles. To keep the circular crack from intersecting with its adjacent circles, the Xia–Hutchinson model pointed out that the pure mode I fracture needs to be maintained with the stress intensity factor of mode II $K_{II} = 0$. Thus, the circular cracks in the present work are dominated by the mode I fracture. In terms of the Xia–Hutchinson model, we have

$$\frac{K_I}{\sigma_0\sqrt{l}} = \sqrt{(1-\nu^2)}\sqrt{\tanh\left(\frac{H}{2l}\right)} \quad (1)$$

dx.doi.org/10.1021/jp301872r | J. Phys. Chem. B 2012, 116, 6225–6231

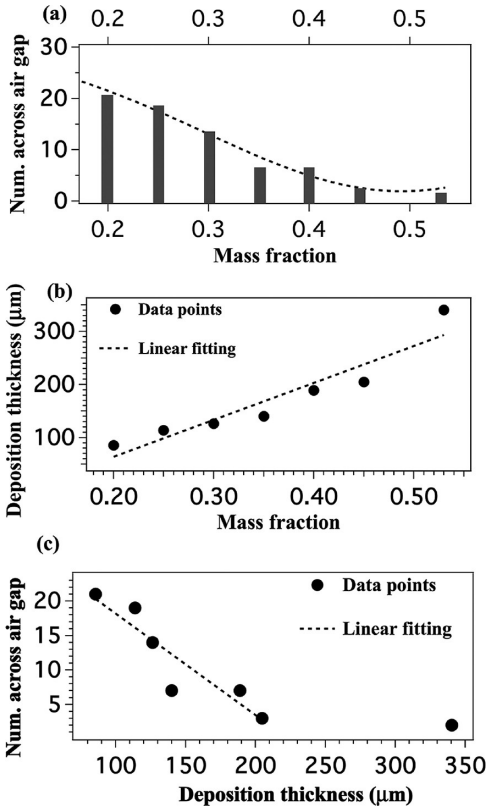

Figure 5. Quantitative correlations among the numbers of cracks across the air gap, the deposition thickness, and the mass fraction of the initial suspension: (a) numbers of crack propagation across air gap falling linearly with the increase of the NP mass fraction; (b) linear dependence of the mean thickness of deposition on NP mass fraction; (c) linear dependence of the numbers of cracks across an air gap on the deposition with thin thickness (less than 200 μm). The dashed line for the mean value in a is the Gaussian fitting.

where K_I is the stress intensity factor, σ_0 the uniform prestress acting normal to the crack line in the deposition, ν Poisson's ratio of the deposition film, and H the distance between the adjacent cracks (as shown in Figure 3h).

l is the reference length given as

$$l = \sqrt{\frac{Eh}{(1-\nu^2)k}} = \frac{\pi}{2} g(\alpha, \beta) h \tag{2}$$

where E and h are Young's modulus and the thickness of the deposition film, respectively, k is the spring constant of the (glass or polystyrene) substrate, and α and β are Dundur's parameters. g is a dimensionless quantity, weakly dependent on β, and mainly designated by α. α can be represented as[17]

$$\alpha = \frac{\overline{E} - \overline{E_s}}{\overline{E} + \overline{E_s}} \tag{3}$$

where $\overline{E} = E/(1-\nu^2)$ and $\overline{E_s} = E_s/(1-\nu_s^2)$ are the plane strain tensile modulus of the deposition film and substrate, respectively, E_s and ν_s are Young's modulus and Poisson's ratio of the substrate, respectively.

The α value ranges from -1 to $+1$, where the negative value of α represents that the film is relatively compliant compared with the substrate, whereas the positive one corresponds to the film much stiffer than the substrate. The elastic modulus E of colloid crystal ranges from 0.01 to 100 Pa,[18] which is far less than that of the substrate (E_s= 3 GPa), accordingly in the present work, $\alpha \approx -1$. Thus the elastic modulus of the deposition film does not affect the α value, and its effect can be neglected.

The corresponding g is about 0.8;[16] from eq 2, we have

$$l = 1.256h \tag{4}$$

The dependence of $K_I/(\sigma_0\sqrt{l})$ and H/l on R/l is plotted in Figure 6 according to eqs 1 and 2. Because σ_0 and l are

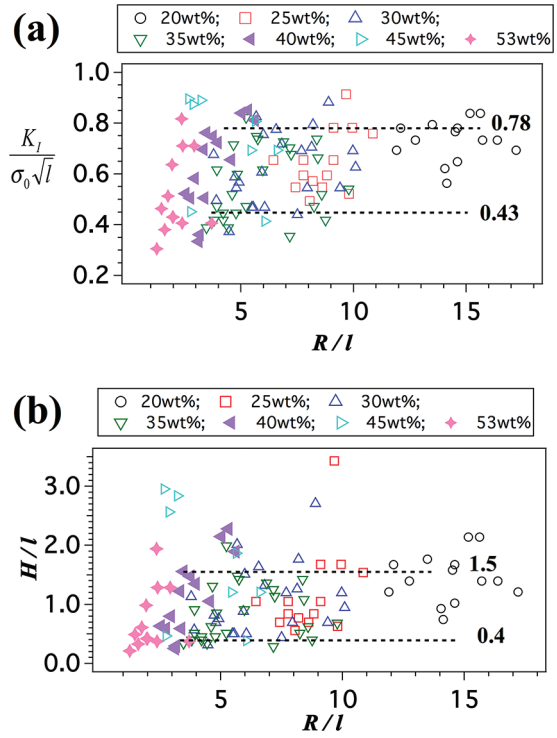

Figure 6. $K_I/(\sigma_0\sqrt{l})$ and H/l versus R/l: (a) stress intensity factor of mode I versus radius of circular crack with various NP mass fractions; (b) distance between two adjacent circular cracks versus radius of circular crack with various NP mass fractions. Error bars of R and H are $\pm$0.01 mm.

constants determined by the material properties, $K_I/(\sigma_0\sqrt{l})$, H/l, and R/l in Figure 6 represent the change of the stress intensity factor, dimensionless circular crack distance, and its radius, respectively. As shown in Figure 6, the values of $K_I/(\sigma_0\sqrt{l})$ and H/l for the NP mass fractions 40 and 53% display generally an upward trend with the increase of R/l, which is consistent with the result in the Xia–Hutchinson model. However, for other NP mass fractions, $K_I/(\sigma_0\sqrt{l})$ and H/l do not exactly rely on R/l, but display nonmonotonic character. The majority of the values of $K_I/(\sigma_0\sqrt{l})$, H/l, and R/l fluctuate in a certain range: from 0.43 to 0.78, from 0.4 to 1.5, and from 2 to 10, respectively, which are close to the values of the work of Xia and Hutchinson. Figure 6 hints at another interesting clue, that large NP mass fractions (40 and 53%) seemly correspond to a small radius for a circular crack, whereas small NP mass fractions (20 and 25%) shift to a large radius.

On the other hand, the energy release rate of a circular crack is lower than that of an isolated straight crack; the ratio is

$$G/G_I = K^2/K_I^2 = \sqrt{\tanh\left(\frac{H}{2l}\right)} \tag{5}$$

dx.doi.org/10.1021/jp301872r | J. Phys. Chem. B 2012, 116, 6225–6231

where G and G_I are the energy release rates of circular and isolated cracks, respectively.

Compared to eq 1, eq 5 only lacks a factor $(1 - \nu^2)^{1/2} = 0.943$. Thus, G/G_I approximately equals $K_I/(\sigma_0\sqrt{l})$ in Figure 6a, and mostly ranges from 46 to 83%. This is consistent with the theoretical prediction. In eq 1, the array of equally spaced cracks in semiinfinite film is mainly considered. The cracks in the deposition can interact across some distance in terms of the Xia–Hutchinson model. This interaction between the cracks lowers the energy release rate of the circular crack.

Xia and Hutchinson stated that it is insufficient to be explained only by the elastic energy release for the curved cracks. The prerequisite condition of the flaw loop needs to be included. The present experimental results first find that the preformed track in dried deposition guides the crack propagation.

B. Impact of Different Deposition Formations on the Crack Trajectories. a. Circular Cracks Prevented by Changing the Formation Condition of Deposition. Because the preformed track closely relates to the deposition microstructure, we further explore the effects on crack trajectory by modifying the formation condition of deposition.

A drop suspension of mass fraction 0.24 dries on the glass substrate. Due to the hydrophilic property of the clean glass, the contact angle and diameter of the drop are 4° and 9.2 mm, respectively. After 3 min evaporating, the drying of the outer region of the disk is complete. One radial crack starts to emerge (Figure 7a), the same as the crack initiation in the section A.a

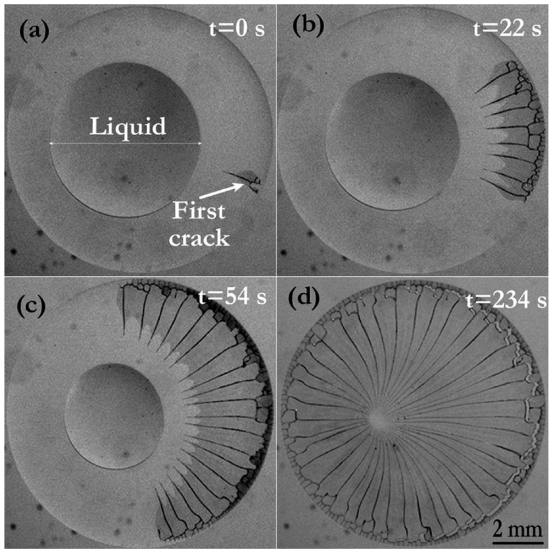

Figure 7. Pattern formation of radius-directional cracks on the glass substrate. Mass fraction of NP suspension: 0.24. (a) A radial direction crack initiates first. (b and c) More and more of the radius-directional cracks occur with the drying proceeding. (d) An entire crack pattern forms as drying is completed. Note that the final drying front is not perfectly located at the center of the spherical cap, mainly due to the slight tilt of the substrate from the perfect horizontal plane. The bar is 2 mm for all micrographs.

(video in the Supporting Information). Water in the drop keeps diffusing into the air, which leads the contact line of the liquid to shrink toward the drop center (Figure 7, Figure 8a). Meanwhile, more cracks appear at the right part of the deposition disk (Figure 7b) and then spread to other areas (Figure 7c). Eventually the radial cracks produce on the whole

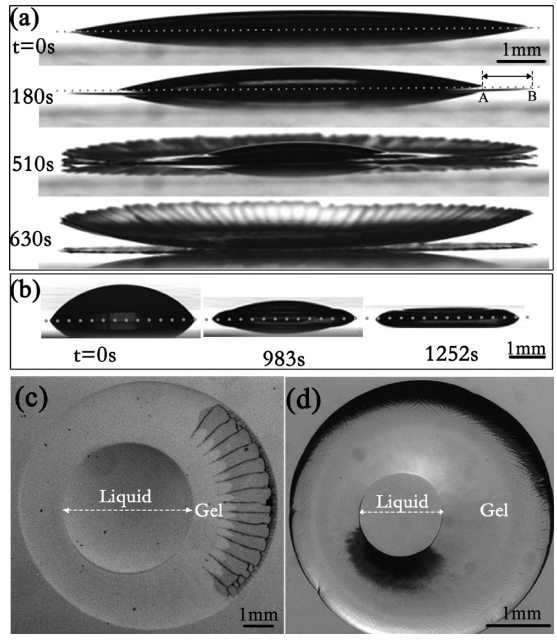

Figure 8. Different stages of drop suspension drying on (side view) (a) hydrophilic glass and (b) hydrophobic polystyrene substrate. The dotted lines in a and b represent the section of the air–substrate interface. (Top view) (c) Cracks for case a with small gelation area; (d) crack-free area with larger gelation for case b during the same stage.

disk as the drying finishes (Figure 7d). The straight cracks separate a certain distance from each other, displaying the periodical distribution which makes up a symmetry pattern. The transition from the circular crack to a radial one means that the crack trajectory is determined by the drying condition for the suspension drops. The following is the analysis of the different deposition microstructures resulting from varying experimental conditions.

b. Hydrodynamics Effect on Deposition Formation. As is well-known, the concentration of the suspension drop increases with continuous evaporating. The ratio of the drying time for drops on the substrates of the glass and polystyrene is $T_r \approx 10$ min/30 min = 0.33:1, which is mainly due to the fact that the evaporation area (surface area of the drop) on the glass is much larger than that on the polystyrene. The drying time has significant effect on the microstructure of the deposition formed by the NP aggregation.

Due to the contact line pinning in the case of the drying on the polystyrene substrate (Figure 8b), the flow from the drop center replenishes the water loss resulting from the higher evaporation rate near the contact line area, which draws the particles toward the contact line and modifies the curvature of the drop surface. Therefore, during the drying process, the height of the drop continually decreases until the drop turns into a thin disk (Figure 8b). Further evaporation leads the suspension to form a gel throughout the deposition. The larger gelation region forms on the disk, and no crack occurs during this gelation (Figure 8d).

However, the contact line on the glass substrate continuously retreats with the drying proceeding (Figure 8a), laying behind the NP deposition. A relatively narrow gelation region is produced between the dried deposition and liquid. Finally, three regions form for the drying on hydrophilic glass: the outmost dried solid region, the liquid region innermost to the

dx.doi.org/10.1021/jp301872r | J. Phys. Chem. B 2012, 116, 6225–6231

center of the drop, and the gelation region between them. The gelation region in the radial direction is very short, immediately following the radial cracks (Figure 8c). As shown in Figure 8a (510 and 630 s), the dried deposited film is delaminated from the substrate as the contact line of the drop is continuously retreating due to the evaporation. The elastic energy stored in the film is released by the delamination[19,20] so that circular cracks have not nucleated in this case. This is significantly different from the drying case on the polystyrene substrate, where the crack does not start to form until gelation is finished. Hereby, during the drying on the polystyrene substrate, the delay for the gelation and the large gelation area finally induce the nucleation of circular cracks.

The difference of the above two depositions is displayed in Figure 8. In the case of drying on the glass substrate with the contact line retreating, a dried deposition film (the section of the film represented by the AB in the micrograph of 180 s in Figure 8a) forms, which is very thin and almost coincides with the substrate interface (dotted line). But for the drying on the polystyrene substrate with contact line pinning, the forming gel leads to a thick deposition disk (the section of disk shown in the micrograph of 1252 s in Figure 8b).

Pauchard et al.[5] achieved the transition from a circular crack to a radial one on the flat glass substrate. Therefore, it infers that the similar crack pattern transition in the present work does not result from the difference of the elasticity mismatch between the glass and polystyrene substrates. Although the similar pattern transitions occur, the intrinsic mechanisms in these two works are fundamentally different. The characteristics of hydrodynamics in the drop and the wettability of the substrates are the key factors ascribing to this transition in the present work, as analyzed in preceding sections, whereas the transition in the Pauchard et al.[5] work was achieved by changing the salt content of the suspension which led to the different gelation time. In addition, the contact angle of the suspension drop on the hydrophilic glass is much smaller than that on the hydrophobic polystyrene. As a consequence, the contact area is larger for the hydrophilic case with the same amount of suspension; i.e., the deposition is thinner. Therefore, more generally, in both works, the crack transition results from the microstructure change for the deposition. Further evidence of deposition microstructure dominating the crack paths is that the formation of crack trajectories is affected by various experimental conditions: the environmental changes (i.e., temperature[21] and humidity[22]), boundary constraints (i.e., shape of the container,[23−25] physical nature of the substrate,[26,27] and so on), and chemical and physical modification of the drying materials (i.e., pH value and ion concentration,[5] film thickness,[9,28] solute type[29,30] and size,[11,31] and extra field introduction[32]). Therefore, the deposition microstructure is the dominant factor for the crack trajectory. To guide the crack propagation on a circular trajectory, the preformed track in the deposition microstructure can mostly be the flaw loop (as proposed by Xia and Hutchinson) where fracture more easily occurs than in the flaw-free areas, in terms of the fracture mechanism.

The roughly visual image of the preformed track can be inferred from Okubo's studies.[33,34] Multiple-ring pattern resulted from the convectional flow during the process of drying colloidal suspension.[33] After the drying finished, the multiple concentric rings were made up by accumulated particles.[33,34] The circle path with less particles produced and lay between the adjacent rings. The preformed track in the present work may have an origin similar to this circle path. The distance between circle paths (ring width in ref 33) increased with the suspension concentration increase, being the same tendency as that of preformed tracks (crack distance in Figure. 4b) in the present work. The accompanying formation of a spokelike (radial) pattern with multiple rings[33] hints at more similarity with the mixture of radial and circular cracks in Figure 2.

Recent research provides the experimental evidence for crack produced on the preformed track in the polymer crystallization.[35] Ring band patterns formed as poly(L-lactic acid) (PLLA) film crystallized at 125 °C. When PLLA was cooled to ambient temperature, ring cracks were produced on the trajectories coinciding with the borders (rings) of crystalline bands in the film. Although this preformed track has not been directly observed in dried NP deposition due to the limitation of current experimental techniques, we have presented the indirect evidence of its existence in the present work.

CONCLUSION

In summary, we study the circular cracks in self-assemble NP deposition induced by drying the suspension drops. We report the first experimental evidence in NP deposition for the predication proposed by the Xia−Hutchinson model: cracks can propagate "across" the air gap along the circular trajectory. Segments of arc crack on several nonconnecting pieces of deposition constitute an entire circular crack trajectory. In addition, two separated arc-path cracks propagate to "meet", constituting the circular trajectory. These results prove that the preformed track leads to the curved trajectory. The transition from the circular crack to a radial one indicates that the unique crack trajectory is determined by the microstructure of the deposition.

ASSOCIATED CONTENT

Supporting Information

Videos showing "CircularPattern", the evolution of the circular for the drying of nanoparticle suspension drop (0.35 of mass fraction) on the polystyrene substrate, and "RadialPattern", the evolution of the radius-directional crack pattern for the drying of nanoparticle suspension drop (0.24 of mass fraction) on the glass substrate. This information is available free of charge via the Internet at http://pubs.acs.org.

AUTHOR INFORMATION

Corresponding Author

*Tel.: (+86) 159 9116 2767. Fax: (+86) 29 8830 2115. E-mail: jing@nwu.edu.cn (G.J.); junma@nwu.edu.cn (J.M.).

Notes

The authors declare no competing financial interest.

ACKNOWLEDGMENTS

The authors gratefully acknowledge the support by NSFC (Grant No. 11104218), the Natural Science Basic Research Plan in Shaanxi Province of China (Program No. 2010JZ001), and the Scientific Research Foundation for the Returned Overseas Chinese Scholars (Shaanxi Administration of Foreign Expert Affairs, 2011).

REFERENCES

(1) Talapin, D. V.; Lee, J. S.; Kovalenko, M. V.; Shevchenko, E. V. *Chem. Rev.* **2010**, *110*, 389−458.

(2) Morag, A.; Philosof-Mazor, L.; Volinsky, R.; Mentovich, E.; Richter, S.; Jelinek, R. *Adv. Mater.* **2011**, *23*, 4327−4331.
(3) Hynninen, A. P.; Thijssen, J. H. J.; Vermolen, E. C. M.; Dijkstra, M.; Van Blaaderen, A. *Nat. Mater.* **2007**, *6*, 202−205.
(4) Moore, E. B.; Molinero, V. *Nature* **2011**, *479*, 506−508.
(5) Pauchard, L.; Parisse, F.; Allain, C. *Phys. Rev. E* **1999**, *59*, 3737−3740.
(6) Wilson, T.; Turner, D. *J. Mater. Sci. Lett.* **1988**, *7*, 875−876.
(7) Sendova, M.; Willis, K. *Appl. Phys. A: Mater. Sci. Process.* **2003**, *76*, 957−959.
(8) Néda, Z.; Leung, K.; Józsa, L.; Ravasz, M. *Phys. Rev. Lett.* **2002**, *88*, No. 95502.
(9) Lazarus, V.; Pauchard, L. *Soft Matter* **2011**, *7*, 2552−2559.
(10) Goehring, L.; Clegg, W. J.; Routh, A. F. *Soft Matter* **2011**, *7*, 7984−7987.
(11) Pauchard, L.; Adda-Bedia, M.; Allain, C.; Couder, Y. *Phys. Rev. E* **2003**, *67*, No. 027103.
(12) Hull, D. *Fractography: Observing, measuring, and interpreting fracture surface topography*; Cambridge University Press: Cambridge, U.K., 1999.
(13) Routh, A. F.; Russel, W. B. *Langmuir* **1999**, *15*, 7762−7773.
(14) Tirumkudulu, M. S.; Russel, W. B. *Langmuir.* **2005**, *21*, 4938−4948.
(15) Russel, W. B.; Wu, N.; Man, W. *Langmuir* **2008**, *24*, 1721−1730.
(16) Xia, Z.; Hutchinson, J. *J. Mech. Phys. Solids* **2000**, *48*, 1107−1131.
(17) Beuth, J.; Klingbeil, N. *J. Mech. Phys. Solids* **1996**, *44*, 1411−1428.
(18) Okubo, T. *J. Colloid Interface Sci.* **1990**, *135*, 259−262.
(19) Sarkar, A.; Tirumkudulu, M. S. *Soft Matter* **2011**, *7*, 8816−8822.
(20) Wallenstein, K.; Russel, W. *J. Phys.: Condens. Matter* **2011**, *23*, No. 194104.
(21) Ye, Y. H.; LeBlanc, F.; Hache, A.; Truong, V. V. *Appl. Phys. Lett.* **2001**, *78*, 52.
(22) Caddock, B.; Hull, D. *J. Mater. Sci.* **2002**, *37*, 825−834.
(23) Li, H. L.; Dong, W.; Bongard, H. J.; Marlow, F. *J. Phys. Chem. B* **2005**, *109*, 9939−9945.
(24) Gauthier, G.; Lazarus, V.; Pauchard, L. *Europhys. Lett.* **2010**, *89*, No. 26002.
(25) Gauthier, G.; Lazarus, V.; Pauchard, L. *Langmuir* **2007**, *23*, 4715−4718.
(26) Groisman, A.; Kaplan, E. *Europhys. Lett.* **1994**, *25*, No. 415.
(27) Cohen, Y.; Mathiesen, J.; Procaccia, I. *Phys. Rev. E* **2009**, *79*, No. 046109.
(28) Shorlin, K. A.; de Bruyn, J. R.; Graham, M.; Morris, S. W. *Phys. Rev. E* **2000**, *61*, No. 6950.
(29) Weh, L.; Venthur, A. *Macromol. Mater. Eng.* **2004**, *289*, 227−237.
(30) Pauchard, L.; Abou, B.; Sekimoto, K. *Langmuir.* **2009**, *25*, 6672−6677.
(31) Kitsunezaki, S. *Phys. Rev. E* **1999**, *60*, No. 6449.
(32) Pauchard, L.; Elias, F.; Boltenhagen, P.; Cebers, A.; Bacri, J. C. *Phys. Rev. E* **2008**, *77*, No. 021402.
(33) Zhao, M. J.; Li, Z. G.; Fei, S. M.; Wang, Z. X. *J. Phys. A: Math. Theor.* **2010**, *43*, No. 275203.
(34) Okubo, T.; Okuda, S.; Kimura, H. *Colloid Polym. Sci.* **2002**, *280*, 454−460.
(35) Nurkhamidah, S.; Woo, E. *Colloid Polym. Sci.* **2012**, *290*, 275−288.